7

Mathematical models of mass transfer in the vascular walls

Karl Perktold, Martin Prosi, and Paolo Zunino

As illustrated in detail in chapters 1 and 2, the arterial wall is a heterogeneous structure consisting of several layers which strongly differ in their thickness and in their biological and physical properties, that we briefly recall here for the sake of clarity. The layers constituting the wall are the *endothelium*, the *intima*, the *internal elastic lamina or lamella* (IEL), the *media* and the *adventitia*, see Fig. 7.1 for a simplified sketch. The endothelium is a type of epithelium composed of a single layer of smooth, thin cells that lines the heart, blood vessels, lymphatics, and serous cavities. It forms a continuous lining on blood contacting surfaces in the vascular system, providing the principal barrier against the entry of cholesterol and blood cells into the wall and inhibiting platelet adherence to the vessel walls. Endothelial cells create chemicals and control the transport of mass into and out of the wall. The sub-endothelial layer is an extra-cellular matrix of randomly distributed fibres, mainly collagenous bundles and proteoglycans (glycoproteins which have a very high polysaccharide content). This layer is surrounded by the IEL, which is composed by elastic fibres. Under normal physiological loading, the fibres form an approximately circular band. Together with the sub-endothelial layer it helps the wall to withstand haemodynamic stresses. Outside the IEL there is the media, which is made of smooth muscle cells and is the primary regulator of vessel diameter. The outer layer is the adventitia, which is a complex structure that merges into the surrounding tissue. It tethers arteries in place and it carries nutrients to and wastes away from smooth muscle cells in the media. Moreover, it provides resistance to overextension and rupture. Sometimes, what we call *intima* is denoted with *sub-endothelial layer*. In this case, the term *intima* is used for the group of endothelium, sub-endothelial layer and IEL. However, we do not follow this nomenclature.

The behaviour and the interaction of these layers are regulated by a complex set of chemical and mechanical phenomena. There is evidence (see [287] for a general introduction or [169] for a more specific analysis) that these mechanisms depend also on fluid dynamics and mass transport phenomena in the blood stream and in the wall. The role of fluid dynamics and mass trans-

Formaggia L, Quarteroni A, Veneziani A (Eds.): Cardiovascular Mathematics. Modeling and simulation of the circulatory system

port processes in the physiological and patho-physiological functions of the vascular system are of great interest. As discussed in Chapter 1, arteriosclerotic disease consists in degenerative changes in the arteries, characterised by thickening of the vessel walls and accumulation of calcium with consequent loss of elasticity and lessened blood flow. Atherosclerosis, in particular, is a common form of arteriosclerosis in which fatty substances form a deposit of plaque on the inner lining of arterial walls. Based on the knowledge that abnormal accumulation of macromolecules such as low density lipoprotein (LDL) or other atherogens in the arterial wall is an important component of the atherosclerotic disease processes, the quantification of the transport phenomena is required. It is world-wide accepted that an improved understanding of vascular mass transport phenomena and the influence of fluid dynamics will have a significant impact on public health.

Atherosclerosis tends to be localised in zones of artery bifurcations and bends where the shearing forces imposed by the flowing blood are disturbed compared with the straight tube patterns ([174, 264]). It has been observed that LDL accumulation in the intima occurring at zones of low and oscillating wall shear stress (in flow separation regions) is associated with the tendency to intimal thickening ([64, 65]). A powerful tool to analyse and quantify the relevant phemomena is computational modelling which provides detailed description of transport features, see [136].

The goals of vascular mass transport studies are to correlate mass transfer in anatomic geometries with the localisation of atherosclerotic lesions and to determine the influence of disturbed flow patterns on the local concentration distribution of substances in the blood stream and in the vessel wall layers. Vascular mass transport analysis requires the development of appropriate mathematical and numerical models. Because of the extreme complexity, the biological problem can be cast with difficulty into a formal physical framework, and simplifications with respect to the real biological situation are unavoidable. Basically the presented analysis is restricted to the dynamics of solutes in large and medium sized arteries. As a consequence, for the specific study of mass transfer blood can be idealised as a *Newtonian fluid* (see for instance [406], [383]). For a more detailed discussion of this assumption, we refer to Chapter 2. Furthermore, rigid arterial walls are assumed, with the justification that for the mass transfer study of large molecules (LDL) from blood to arterial walls accounting for wall displacement is not crucially important. However, for small molecules (oxygen), the wall compliance affects the flux into the wall significantly, see [399]. The application of mass and momentum conservation laws under these assumptions comes up to the incompressible *Navier-Stokes equations* (see Chapter 2). According to the fact that blood plasma filtrates from the inner to the outer part of the arterial walls under the action of blood pressure, it will be necessary to model the fluid flow in the wall layers, considered to be homogeneous porous media. In this case the conservation laws describing the plasma filtration lead to the *Darcy or Darcy-Brinkman equation*. Moreover, recent experiences show that

intra-cellular transport also plays a role in the mass transfer through the arterial walls ([491] and references therein). Regarding the solute dynamics the limitation to consider the presence of just one solute is applied. Moreover, according to physical evidence, the concentration of chemicals dissolved in blood is small; consequently the blood motion is not influenced by chemicals. Then, by virtue of the mass conservation principle, the concentration of the considered solute is governed by a classical *advection-diffusion equation*.

Several mathematical models have been developed recently for the study of the transport of macromolecules (such as LDL) in arteries e.g., [249, 397, 476, 533, 563]). Essentially, the models can be classified in three categories corresponding to the level of description of the arterial wall.

For the simplest model, the *wall-free* model, the arterial wall is described by means of an appropriate boundary condition at the inner surface of the artery (lumen-endothelial boundary). The appropriate boundary conditions depend on the considered molecules. The transfer of *dissolved gases* (small molecules, e.g., oxygen) to and into the wall is diffusion boundary layer controlled, because of the fact that the endothelium is not an essential barrier to these molecules. The assumption of a constant concentration at this boundary is justified. Originally, this model was applied for the study of arterial oxygen concentration by [20, 132, 421]. The main resistance to the transfer of *macromolecules* from lumenal blood into the arterial wall is the endothelial layer. The flux across the endothelium into the inner layers of the arterial wall is determined by the endothelial permeability and by the concentration differential across the layer. Therefore, the permeability boundary condition (which is of Robin type) can be applied. The model requires the prescription of the concentration in the sub-endothelial intima. This model needs a relatively small number of parameters, the diffusivity, the overall mass transfer coefficient of the wall and the filtration velocity. The model was applied to analyse the local concentration of potentially atherogenetic molecules by [305] (ATP), by [533] (LDL). The model cannot provide any information on the concentration of solute within the wall, however, concentration polarisation effects in the blood phase directly at the wall can be addressed accurately.

Improved developments, the *fluid-wall* models, account for the arterial wall, where the mass transport in blood and in the wall are described applying physically appropriate laws to model the interaction between the blood flow and the biochemical transport. In the first stage of improvement the complex physiologic heterogeneous wall structure is approximated by one homogeneous porous layer representing the media. This layer is separated from the lumen by a membrane, which corresponds to the three physiologic layers endothelium, intima and IEL. The transport processes in the blood stream (lumen) and in the wall are coupled applying appropriate membrane equations. This model is well suited to describe the dynamics of solutes in healthy arteries, where the intima is a very thin layer, and the endothelium represents the main resistance to the solid. The most complex arterial transport model proposed so far is the *multilayer* model, which takes into account for the several heterogeneous

layers, endothelium, intima, IEL and media (see [175, 176] for its definition; [58,563] for the analysis of existence and uniqueness of solutions; [249,251] for the analysis of a finite element scheme applied to this case). The multilayer model provides the most realistic information on the dynamics of chemicals (macromolecules) in the wall. The physical behaviour of the different layers are approximated with the laws of mass transport in homogeneous porous media (intima and media) and through plasma-permeable membranes (endothelium and IEL).

7.1 Governing equations for mass transfer in the cardiovascular system

The mathematical modelling for mass transfer in the cardiovascular system originated from the study of microcirculation with the aim to provide models for the mass transfer through the capillaries. Basic references are Friedman [173], Katchalsky and Curran [254] and for the specific application to the vascular system we mention Curry [106]. These works mainly neglect the space dependence of the quantities of interest because of the geometrical complexity of the capillary network. According to this tendency, we start our work with the study of two solutions of one single chemical whose concentration is small and uniform and we address in this setting the basic principles of transport processes. Then, we present the general lines to set up a mathematical model for mass transfer through the arterial walls. This procedure applies either to the wall-free, fluid-wall and multilayer model. Finally, we focus our attention on the multilayer model, which deserves a detailed discussion because of its complexity.

7.1.1 Principles of transport processes

We consider two solutions that are separated by a porous thin membrane that allows the flux of both solvent and solute from one compartment to the other. The membrane is not totally transparent with respect to the transport of mass, and makes a selection between the molecules that can pass through its interstices and those that can not. Membranes featuring this behaviour are called *selective permeable membranes*. As it will be made clear in the following paragraphs, these phenomena typically happen between the lumen and the wall or between the different layers of the wall.

Given a semipermeable membrane separating two solutions of concentration c in a suitable solvent, we denote with J_v the filtration velocity of the solvent across the membrane and with J_s the mass flux of the chemical per unit surface. Let L_p and $\mathcal{P}$ the hydraulic conductivity and the permeability of the membrane. The sieving coefficient, denoted with s, determines the ratio of molecules that can sieve across the membrane. In what follows we will also use the reflection coefficient that is the complementary of s with respect to

the unity. We denote the reflection coefficient with $\sigma = 1 - s$. We will consider two different kind of reflection and sieving coefficients, the osmotic one (also called solvent drag sieving coefficient), denoted with $\sigma_d = 1 - s_d$ and the frictional one $\sigma_f = 1 - s_f$. Finally, the index $i = 1, 2$ denotes here the two compartments separated by the semipermeable membrane.

A well accepted mathematical model for the fluxes of solvent and the solute is given by the following set of equations, called *Kedem-Katchalsky* equations (see for example [254, 255]).

$$J_v = L_p(\delta p - \sigma_d \delta \pi) \tag{7.1}$$

$$J_s = \mathcal{P}\delta c + J_v(1 - \sigma_f)\overline{c}, \tag{7.2}$$

where $\overline{c}$ is the mean concentration inside the membrane and $\delta c = c_1 - c_2$, $\delta p = p_1 - p_2$, while

$$\delta \pi = RT\delta c, \tag{7.3}$$

where R, T are the gas constant and the absolute temperature. Equation (7.1) is called Starling's law of filtration and states that the solvent flux across the membrane is proportional to the pressure jump between the two compartments. The pressure jump is, on the other hand, split in two parts, the jump of static pressure δp and the jump of osmotic pressure $\delta \pi$. The latter depends on the solute concentration on the two sides of the membrane, according to the Van't Hoff's law (7.3). On the other hand, the solute flux, defined by equation (7.2), can be interpreted as the sum of a diffusive term (depending on the jump of concentration across the membrane) and a transport term (defined as the product of effective solvent flux and the mean concentration within the membrane). From another point of view, system (7.1,7.2) can be interpreted as the description of the influence of the driving forces acting through a membrane, namely δp and δc on the physical quantities J_v, J_s. The parameters $L_p, \mathcal{P}$ are the coefficients that govern this dependence and are called *phenomenological coefficients*.

A very delicate parameter appearing in the Kedem-Katchalsky equations is the average concentration within the membrane ($\overline{c}$). In fact, several models can be considered to estimate this quantity starting from physical considerations.

Let us assume that the dynamics of solute within the membrane are governed by diffusion and transport. Precisely, the concentration within the membrane satisfies the following boundary-value problem,

$$\begin{aligned} &-ac''(x) + bc'(x) = 0, \quad x \in (0, l) \\ &c(0) = c_1, \quad c(l) = c_2, \end{aligned} \tag{7.4}$$

where the cross-section of the membrane is represented by the interval $(0, l)$ while the coefficients $a := \mathcal{P}$ and $b := L_p(1 - \sigma_f)(p_1 - p_2)$ take into account the diffusion and the transport respectively. Finally c_1 and c_2 represent the concentration on the sides of the membrane. The solution of problem (7.4) is,

$$c(x) = \frac{1}{1 - \exp(Pe)} \left[c_2 - \exp(Pe)c_1 + (c_1 - c_2) \exp\left(\frac{bx}{a}\right) \right], \quad x \in (0, l),$$

where we have introduced the *global Péclet number* associated with problem (7.4), $Pe := bl/a$. Then the average concentration within the membrane, defined as $\overline{c} := (1/l)\int_0^l c(x)dx$ becomes,

$$\overline{c} = f_w(c_1, c_2) = w_1 c_1 + w_2 c_2$$

$$w_1 = \frac{\exp(Pe)}{\exp(Pe) - 1} - \frac{1}{Pe}, \quad w_2 = \frac{1}{Pe} - \frac{1}{\exp(Pe) - 1}.$$

In what follows, we call $f_w(c_1, c_2)$ the weighted arithmetic average. For example, let us consider this average for a membrane representing the endothelium. Thus, we set $l = 10^{-4}$cm, $\mathcal{P} = 10^{-7}$cm/s, $a = 10^{-11}$cm^2/s and $b = 10^{-6}$cm/s (the latter provides a reasonable approximation for the filtration velocity in the wall). The solute dynamics in the endothelium are in this case transport dominated (indeed, the Péclet number is high, $Pe = 100$) and we obtain $w_1 = 0.99, w_2 = 0.01$. This choice of the average concentration $\overline{c}$ is appropriate for membranes whose thickness is considerable with respect to the characteristic size of the molecules that filtrate through them.

An alternative approach to determine the average concentration within the membrane makes use of irreversible thermodynamics, the Kedem-Katchalsky equations can be theoretically derived from the general Onsager's phenomenological equations (see for example [254] Chapter 8), by applying them to the study of mass transport through membranes. For this matter the interested reader is referred to [173, 254, 255]. In this framework, the average concentration within the membrane can be defined starting from the Nerst-Planck equation for equilibrium of chemical potentials and it becomes $\overline{c} = f_l(c_1, c_2) = (c_1 - c_2)/\ln(c_1/c_2)$, which we call logarithmic average. Physical experience suggests that this model is suitable for extremely thin selective permeable membranes.

It is straightforward to verify that these models lead to different values of the average concentration. For example, in the common case of highly resistant membranes and of solute exchange dominated by transport, one has $c_1/c_2 \gg 1$ as well as $Pe \gg 1$, which leads to $f_w(c_1, c_2) \simeq c_1$ while $f_l(c_1, c_2) \simeq 0$. On the other hand, we observe that if the solute dynamics within the membrane is dominated by diffusion and the membrane is very permeable, one has $c_1/c_2 \simeq 1$ and $Pe \simeq 1$, which leads to $f_l(c_1, c_2) \simeq f_w(c_1, c_2) \simeq 1/2(c_1 + c_2)$. Finally, we observe that in the general case, the concentration within the membrane will be denoted as $\overline{c} = f(c_1, c_2)$.

7.1.2 Set up of the multilayer model

The starting point of this section is the description of the blood flow into the arterial lumen. It is governed by the Navier-Stokes equations, which are extensively discussed in Chapter 3 (see in particular equations (3.32) and (3.40)).

Concerning the arterial wall, we remind that in any biological tissue flow may take place through a complex network of interconnected pores, or openings. However, when dealing with such flow, we overlook the microscopic flow patterns inside individual pores and we consider some fictitious average which takes place in the porous medium comprising the tissue. By doing so, we are employing the concept of a continuum, which is common in most branches of physics. The obvious reason for employing the continuum approach in flow through a porous medium, is that it is practically impossible to describe in any exact mathematical manner the complicated geometry that bounds the flowing fluid. In order to set up the mathematical models for flow in porous media based on the continuum approach, we introduce the porosity of the tissue, $0 < \epsilon < 1$, and its hydraulic permeability (or Darcy permeability), K_D, which is assumed here to be a constant scalar quantity. In the case of a free fluid we set $\epsilon = 1$. We denote with $\boldsymbol{u}$ the volume averaged velocity and with $\tilde{\boldsymbol{u}}$ the velocity of the fluid phase. Similar notations, c and $\tilde{c}$, are adopted for the concentration of chemical dissolved in the solution permeating the tissue. We notice that the ratio between volume averaged value of a physical quantity and the value of the corresponding quantity in the fluid phase is given by $\epsilon = \boldsymbol{u}/\tilde{\boldsymbol{u}} = c/\tilde{c}$.

Under the assumption that blood plasma completely fills the void space of the porous medium, we consider two options to describe the average fluid flow into the tissue, the Darcy's model and the Brinkman's model. Both the Darcy's and the Brinkman's equations can be derived by means of homogeneisation techniques starting from the Stokes flow through an array of particles (for a detailed discussion we refer for example to [283]). Moreover, the Brinkman's model can be regarded as a correction of the Darcy's one featuring a viscous term inspired from the Stokes equations. The Darcy's model reads as follows,

$$\boldsymbol{u} = -\frac{K_D}{\mu}\boldsymbol{\nabla} p \quad \text{with} \quad \mathbf{div}\boldsymbol{u} = 0,$$

while the Brinkman's model is given by,

$$\boldsymbol{u} = -\frac{K_D}{\mu}[\boldsymbol{\nabla} p - \mu'(\nabla \boldsymbol{u} + \nabla \boldsymbol{u}^T)], \quad \mathbf{div}\boldsymbol{u} = 0,$$

where μ' is called the Brinkman's modified viscosity. Finally, the dynamics of chemicals is governed by a system of advection-diffusion equations. Precisely, applying the mass conservation principle on a generic control volume, we obtain the following equation

$$\partial_t c + \mathbf{div}(-D\boldsymbol{\nabla} c + \gamma \boldsymbol{u} c/\epsilon) = 0. \tag{7.5}$$

We observe that collisions of large molecules with the structure of the porous tissue layer result in a reduced convective transport. This phenomenon is taken into account by using a hindrance coefficient $0 < \gamma \leq 1$ in the mathematical model (see below).

In the wall-free model the fluid dynamics and the mass transport in the arterial lumen are described by the Navier-Stokes equations and the advection-diffusion equations. At the boundary between the lumen and the arterial wall appropriate conditions for the volume flux (J_v) and the mass flux (J_s) are assumed,

$$\begin{aligned} \boldsymbol{u}_l \cdot \boldsymbol{n}_l &= J_v \quad \text{on} \quad \Gamma \\ (-D_l \nabla c_l + \boldsymbol{u}_l c_l) \cdot \boldsymbol{n}_l &= J_s \quad \text{on} \quad \Gamma. \end{aligned}$$

In this case the values of J_v and J_s are provided by experimental data in [49, 492, 513, 533]. In the case of the fluid-wall model and the multilayer model we need suitable matching conditions between the governing equations in different media. These conditions are provided by the Kedem-Katchalsky equations (7.1)–(7.2) and their application will be presented in detail for the multilayer model in what follows.

To set up the multilayer model, first of all we recall that the arterial wall consists of the endothelium (whose thickness is of the order of 2 µm), intima (thickness $\simeq$ 10 µm), internal elastic lamina (IEL, thickness $\simeq$ 2 µm), media (thickness $\simeq$ 300 µm) and adventitia. In the latter layer, pressure and the concentration are supposed to be known from measurements. In order to reduce the complexity of the resulting numerical problem, some simplifications are in order. An approach, proposed and discussed in [411, 420, 421], consist of treating the thinner layers as membranes through the Kedem-Katchalsky equations, see e.g. (7.1,7.2). Consequently the problem that we address here features three coupled domains: the lumen, the intima, the media, separated by interfaces, representing the endothelium and the IEL. A representation of the domains is given in Fig. 7.1. In order to set up the equations of the model,

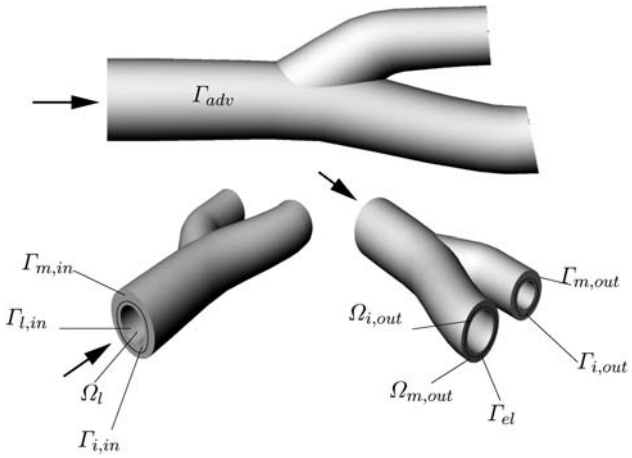

Fig. 7.1. The considered domains and the partitioning of the boundaries for the multilayer model

we will denote with the subscripts l, i, m the physical quantities related with the lumen, the intima and the media respectively. Moreover, we will apply the subscripts *end* and *iel* for the endothelium and the internal elastic lamina.

Fluid dynamics models

In order to find out whether the Darcy's or the Brinkman's model is more suited to our purpose, we focus on the interface conditions between the lumen and the wall, corresponding to the endothelial layer denoted with Γ_{end}. We notice that on the lumenal side we consider the interface as a non-slip surface that only allows normal flow. On the other hand, since the Darcy model does not allow any control on the tangential velocity on the boundary, there might be a discontinuity of it across Γ_{end}. Although, this is not likely to happen because the flow in the wall is driven by the pressure jump $p_l - p_{adv}$ and is mainly radial, the Darcy-Brinkman model is able to override this drawback. In fact it can be supplemented by conditions enforcing the continuity of the velocity across interfaces, since it features a viscous term. In general these conditions seem to be more realistic than the ones imposed in the Darcy case. However, we observe that the tangential velocity on the lumen-wall interface rapidly goes to zero into the wall. A rough estimation of the boundary layer thickness can be computed as in [445]. Assuming that the wall is characterised by the following parameters

- diameter of the pores, $D_p = 30\text{nm} = 30 \cdot 10^{-9}\text{m}$;
- porosity of the wall, $\epsilon = 0.96$;
- channel thickness, $H = 1\text{cm}$;
- permeability of the wall $K_i = [D_p^2 \epsilon^3]/[150(1-\epsilon)^2] = 0.33 \cdot 10^{-14}\text{m}^2$,

the boundary layer thickness δ is then,

$$\delta = K_i^{1/2} \log \left[50(h/K_i^{1/2} - 1) \right] = 9.2 \cdot 10^{-7}\text{m} \simeq 1\,\mu\text{m}.$$

We observe that the thickness of the boundary layer is half the thickness of the endothelium (about $2\,\mu\text{m}$). Furthermore, we point out that in the multilayer model the endothelium and the internal elastic lamina are treated as membranes, due to their extremely small thickness. Consequently, the Darcy-Brinkman model does not look fully consistent with the multilayer model since, in order to be correctly applied, it could require us to resolve details on a scale that is smaller than the thickness of the endothelium or the internal elastic lamina. Hence the Navier-Stokes/Darcy coupling looks more suitable in our case. Then, the system including the Navier-Stokes and the Darcy's equations (where we use the previously introduced notation) reads as flows.

$$J_{v,end} = L_{p,end}(p_l - p_i) - L_{p,end}\sigma_d RT(c_l - c_i) \text{ on } \Gamma_{end}, \tag{7.6}$$

$$J_{v,iel} = L_{p,iel}(p_i - p_m) - L_{p,iel}\sigma_d RT(c_i - c_m) \text{ on } \Gamma_{iel}. \tag{7.7}$$

Problem 7.1.1 Find the velocities and pressures in the lumen, intima and media $\boldsymbol{u}_l, p_l$, $\boldsymbol{u}_i, p_i$, $\boldsymbol{u}_m, p_m$, respectively, such that

$$
\begin{aligned}
&(a)\ \frac{\partial \boldsymbol{u}_l}{\partial t} + (\boldsymbol{u}_l \cdot \nabla)\boldsymbol{u}_l - \mathbf{div}\boldsymbol{\sigma}_l/\rho = \mathbf{0} \quad \text{in } \Omega_l, \quad t > 0 \\
&(b)\ \mathbf{div}\boldsymbol{u}_l = 0 \quad \text{in } \Omega_l, \quad t > 0 \\
&(c)\ \boldsymbol{u}_l = \boldsymbol{u}_{l,in} \quad \text{on } \Gamma_{l,in}, \quad t > 0 \\
&(d)\ \boldsymbol{\sigma}_l \boldsymbol{n}_l = p_{out}\boldsymbol{n}_l \quad \text{on } \Gamma_{l,out}, \quad t > 0 \\
&(e)\ \boldsymbol{u}_l \times \boldsymbol{n}_l = \mathbf{0}, \quad \boldsymbol{u}_l \cdot \boldsymbol{n}_l = \boldsymbol{u}_i \cdot \boldsymbol{n}_l \quad \text{on } \Gamma, \quad t > 0 \\
&(f)\ \boldsymbol{u}_l = \boldsymbol{u}_0 \quad \text{with} \quad \mathbf{div}\boldsymbol{u}_0 = 0 \quad \text{in } \Omega_l,
\end{aligned}
\tag{7.8}
$$

(where $\boldsymbol{\sigma}_l$ is the Cauchy stress tensor defined in equation (3.33). Condition (7.8_e) states that Γ is a no-slip boundary that allows for filtration in the normal direction. Moreover, we require the normal velocity component across Γ to be continuous)

$$
\begin{aligned}
&(a)\ \boldsymbol{u}_i + \tfrac{K_i}{\mu_i}\boldsymbol{\nabla} p_i = 0 \quad \text{in } \Omega_i, \quad t > 0, \\
&(b)\ \mathbf{div}\boldsymbol{u}_i = 0 \quad \text{in } \Omega_i, \quad t > 0, \\
&(c)\ \boldsymbol{u}_i \cdot \boldsymbol{n}_i = 0 \quad \text{on } \Gamma_{i,in} \cup \Gamma_{i,out}, \quad t > 0, \\
&(d)\ \boldsymbol{u}_i \cdot \boldsymbol{n}_i = -J_{v,end} \quad \text{on } \Gamma_{end}, \quad t > 0, \\
&(e)\ \boldsymbol{u}_i \cdot \boldsymbol{n}_i = J_{v,iel} \quad \text{on } \Gamma_{iel}, \quad t > 0,
\end{aligned}
\tag{7.9}
$$

(equation (7.9_a) is the Darcy's law of filtration with a constant and scalar Darcy's permeability, K_i. Equation (7.9_b) accounts for the conservation of mass. Boundary condition (7.9_c) enforces the filtration velocity to be tangential to the distal and proximal sections of the wall. Conditions ($7.9_{d,e}$) determine the value of the filtration velocity into the endothelium and the IEL according to the Kedem-Katchalsky equations (7.1),(7.2))

$$
\begin{aligned}
&(a)\ \boldsymbol{u}_m + \tfrac{K_m}{\mu_m}\boldsymbol{\nabla} p_m = 0 \quad \text{in } \Omega_m, \quad t > 0, \\
&(b)\ \mathbf{div}\boldsymbol{u}_m = 0 \quad \text{in } \Omega_m, \quad t > 0, \\
&(c)\ \boldsymbol{u}_m \cdot \boldsymbol{n}_m = 0 \quad \text{on } \Gamma_{m,in} \cup \Gamma_{m,out}, \quad t > 0, \\
&(d)\ \boldsymbol{u}_m \cdot \boldsymbol{n}_m = -J_{v,iel} \quad \text{on } \Gamma_{iel}, \quad t > 0, \\
&(e)\ p_m = p_{adv} \quad \text{on } \Gamma_{adv}, \quad t > 0,
\end{aligned}
\tag{7.10}
$$

(equations ($7.10_{a,b}$) and conditions ($7.10_{c,d}$) are analogous to the ones set for the intima. Condition (7.10_e) fixes the pressure value on the adventitia to a known value p_{adv}). □

Finally, we point out that it is still possible account for the shear phenomena in the tangential direction on the fluid-wall interface. This is achieved by a special matching condition applied to the fluid side, proposed at first by Beavers and Joseph and generalised by Jones (see [445]). This condition reads as follows,

$$\frac{K_i^{1/2}}{\mu_i}\left[(\boldsymbol{\sigma}_l \boldsymbol{n}_l)\times \boldsymbol{n}_l\right] = \left(\frac{\mu_i'}{\mu_i}\right)^{1/2}\left[\boldsymbol{u}_l \times \boldsymbol{n}_l - \boldsymbol{u}_i \times \boldsymbol{n}_l\right] \quad \text{on } \Gamma. \tag{7.11}$$

Indeed, (7.11) states that the shear stress on the fluid-wall interface induces a jump on the tangential velocity across the interface. This boundary condition looks particularly suitable in our case, since it takes into account the variation of the tangential velocity across the endothelium, still represented as a membrane.

Solute dynamics models

First of all, we remind that because of friction phenomena on the motion of molecules, the actual transport velocity in the wall is smaller than the filtration velocity obtained from Problem 7.1.1. Consequently, we denote the transport field in equations (7.15,7.16) as an *effective* velocity, given by $(\gamma_\lambda/\epsilon_\lambda)\boldsymbol{u}_\lambda), \lambda = i, m$, where γ_λ is a constant called *friction or hindrance coefficient*, as in equation (7.5). For a more detailed discussion of this issue, we refer to [138, 249, 251]. Furthermore, we rewrite equation (7.2) with a general mean concentration within the membrane that we denote with $f(\cdot,\cdot)$:

$$J_{s,end} = \mathcal{P}_{end}(c_l - c_i) + L_{p,end}(1-\sigma_f)(p_l - p_i)f(c_l, c_i) - L_{p,end}(1-\sigma_f)\sigma_d RT f(c_l, c_i)(c_l - c_i), \tag{7.12}$$

$$J_{s,iel} = \mathcal{P}_{iel}(c_i - c_m) + L_{p,iel}(1-\sigma_f)(p_i - p_m)f(c_i, c_m) - L_{p,iel}(1-\sigma_f)\sigma_d RT f(c_i, c_m)(c_i - c_m). \tag{7.13}$$

Then, making use of these definitions, we propose the following problem for the solute dynamics.

Problem 7.1.2 Find the concentrations in the lumen, intima and media c_l, c_i, c_m respectively such that,

$$\begin{aligned}
&\frac{\partial c_l}{\partial t} + \mathbf{div}(-D_l \boldsymbol{\nabla} c_l + \boldsymbol{u}_l c_l) = f_l,\ t>0,\ c_l(0) = c_{l,0} \text{ in } \Omega_l,\\
&(a)\quad c_l = c_{l,in} \text{ on } \Gamma_{l,in},\ t>0\\
&(b)\quad \boldsymbol{\nabla} c_l \cdot \boldsymbol{n}_l = 0 \text{ on } \Gamma_{l,out},\ t>0\\
&(c)\quad -D_l \boldsymbol{\nabla} c_l \cdot \boldsymbol{n}_l + \boldsymbol{u}_l \cdot \boldsymbol{n}_l c_l = J_{s,end} \text{ on } \Gamma_{end},\ t>0,
\end{aligned} \tag{7.14}$$

(condition (7.14_c) that determines the solute flux across Γ_{end} according to theKedem-Katchalsky equations. Moreover, we refer to Fig. 7.1 for the definitions concerning the boundary partition)

$$\begin{aligned}
&\frac{\partial c_i}{\partial t} + \mathbf{div}(-D_i \boldsymbol{\nabla} c_i + \frac{\gamma_i}{\epsilon_i} \boldsymbol{u}_i c_i) + r_i c_i = f_i,\ t > 0, c_i(0) = c_{i,0} \text{ in } \Omega_i, \\
&(a) \quad \boldsymbol{\nabla} c_i \cdot \boldsymbol{n}_i = 0 \text{ on } \Gamma_{i,in} \cup \Gamma_{i,out},\ t > 0, \\
&(b) \quad - D_i \boldsymbol{\nabla} c_i \cdot \boldsymbol{n}_i + \tfrac{\gamma_i}{\epsilon_i} \boldsymbol{u}_i \cdot \boldsymbol{n}_i c_i = -J_{s,end} \text{ on } \Gamma_{end},\ t > 0, \\
&(c) \quad - D_i \boldsymbol{\nabla} c_i \cdot \boldsymbol{n}_i + \tfrac{\gamma_i}{\epsilon_i} \boldsymbol{u}_i \cdot \boldsymbol{n}_i c_i = J_{s,iel} \text{ on } \Gamma_{iel},\ t > 0,
\end{aligned} \tag{7.15}$$

(we introduced into the governing equations the term $r_i c_i$ accounting for consumption of chemicals by the tissues constituting the intima. Condition (7.15_a) enforces a null diffusive flux on the proximal and distal section of the intima. Condition ($7.15_{b,c}$) enforce on Γ_{end} and Γ_{iel} the flux prescribed by the Kedem-Katchalsky equations)

$$\begin{aligned}
&\frac{\partial c_m}{\partial t} + \mathbf{div}(-D_m \boldsymbol{\nabla} c_m + \frac{\gamma_m}{\epsilon_m} \boldsymbol{u}_m c_m) + r_m c_m = f_m,\ t > 0\ c_m(0) = c_{m,0} \text{ in } \Omega_i, \\
&(a) \quad c_m = c_{adventitia} \text{ or } \boldsymbol{\nabla} c_m \cdot \boldsymbol{n}_m = 0 \text{ on } \Gamma_{adv},\ t > 0, \\
&(b) \quad \boldsymbol{\nabla} c_m \cdot \boldsymbol{n}_m = 0 \text{ on } \Gamma_{m,in} \cup \Gamma_{m,out},\ t > 0 \\
&(c) \quad - D_m \boldsymbol{\nabla} c_m \cdot \boldsymbol{n}_m + \tfrac{\gamma_m}{\epsilon_m} \boldsymbol{u}_m \cdot \boldsymbol{n}_m c_m = -J_{s,iel} \text{ on } \Gamma_{iel},\ t > 0.
\end{aligned} \tag{7.16}$$

(the governing equation and the boundary conditions for the media are analogous to the ones prescribed for the intima). □

In conclusion, Problems 7.1.1 and 7.1.2 represent the multilayer model for mass transfer across the arterial wall. Besides its technical complexity, its definition presents some intrinsic difficulties that appear both in the mathematical analysis of the well posedness of the problem and in its numerical approximation.

On one hand, we observe that Problems 7.1.1 and 7.1.2 are coupled by the interface conditions based on the fluxes $J_{v,end}$, $J_{v,iel}$ and $J_{s,end}$, $J_{s,iel}$ that contain terms involving both the pressure and the concentration. We want to simplify this situation. Since our aim is to study the absorption of macromolecules in the arterial wall, we avoid any simplification on the solute dynamics model, rather we make some assumptions on the equations concerning the blood flow. We obtain a simplification dropping in equations (7.6, 7.7) the term depending on the concentration. More precisely, by taking $J_{v,end} = L_{p,end}(p_l - p_i)$ on Γ_{end} and $J_{v,iel} = L_{p,iel}(p_i - p_m)$ on Γ_{iel}, as *reduced solvent fluxes*, equations (7.9,7.10) do not depend on the concentration, so they can be rewritten with the pressure as an unknown. On the other hand, the coupling between subequations of problems 7.1.1 and 7.1.2 will be approached in Section 7.3 in the framework of the numerical approximation of the multilayer model.

These difficulties also make the mathematical analysis of the coupled Problems 7.1.1 and 7.1.2 an extremely challenging task. Indeed, this is still an open issue. Indeed, we observe that the expressions of $J_{s,end}$, $J_{s,iel}$ are nonlinear functions of the concentrations. This is a major difficulty in the analysis of the well posedness and of the mathematical properties of the model 7.1.2, even when it is split from 7.1.1. We will not dwell here with a complete treatment of these topics, but we point out that the relevance of the analytical study with respect to the aim of this work is twofold. On one side, existence and uniqueness of a solution are the basic properties that have to be satisfied by mathematical models representing physical phenomena. These properties make also possible to consider the numerical approximation of the problem and to compute its solution by numerical methods. In addition to this, if the solution of the original problem is regular enough, the analysis of accuracy of the numerical method can be pursued (see for example Section 7.3). On the other side, the analysis of other specific mathematical properties, as for instance the maximum principle, allows us to characterise more precisely the behaviour of the solution. To sum up, the mathematical analysis provides a synthetic description of the multilayer model that turns out to be very useful in the applications, for example for the interpretation of the numerical results.

Remark 7.1.1 (Mathematical analysis) *Properties as existence, uniqueness and maximum principles have been widely investigated for standard elliptic operators, see e.g. [192], and in the parabolic case, in particular for advection diffusion problems in [398] or [471]. However, we point out that the multilayer model can not be casted into the classical framework, because of the non standard, non linear boundary or matching conditions on the interface between lumen and wall. In the linear case, the analysis of the model has been pursued in [411]. In the non linear case, existence and uniqueness results have been obtained in [58]. However, many analytical issues are still open. For instance, the solution of the multilayer problem may blow up in finite time. The study of blow up is a peculiar topic in analysis of partial differential equations for which we refer to [24] and [87] for a general introduction and to [152, 153, 280, 281] for analytical results that fit our case.*

7.2 Characterisation of physiological data

The physiological correct set up of the mathematical model for the lumenal and transmural fluid and solute dynamics needs appropriate transport parameters. These parameters describe the transport properties of the domains considered in the model (lumen, endothelium, intima, IEL and media). Many of these parameters can not be gained directly by experimental measurements. In this chapter we will discuss two possible mathematical methodologies developed to obtain a complete set of parameters for the different kinds of wall layers (membranes and fibre layers). The first part focuses on

the estimation by using the pore theory that bases on the assumption that the wall layers are porous structures whose physical properties can be identified by their geometrical structure. This kind of method has been proposed in [11, 106, 233, 234, 270]. The majority of this part has been take from [251] where these models have been applied to obtain all parameters of the heterogenous wall structure. The second part describes a different kind of approach by a simplified inverse model based on an electrical analogy for the transport processes. The derivation of the electrical analogies for membranes and porous structers and their application to the arterial wall has been described in detail in [397].

7.2.1 Pore theory

Mass transport in the porous intima and media

The healthy subendothelial intima and the media generally consist of an extracellular matrix of randomly distributed proteoglycan and collagen fibres. In the media, as well as in the thickened intima smooth muscle cells occur in addition to the fibrous fluid phase. The transport processes in these arterial wall layers only occur in the fluid phase.

The fibre matrix is characterised by the wall layer thickness H, the fibre radius r_f and by the total length of the fibres l_f within the unit volume. Hence the fractional void volume of the fibre matrix results from,

$$\epsilon_f = 1 - \pi r_f^2 l_f.$$

The Darcy permeability $K_{D,f}$ of the porous tissue is given as,

$$K_{D,f} = \frac{r_f^2 \epsilon_f^3}{4G(1-\epsilon_f)^2}, \tag{7.17}$$

where G is the Kozeny constant, [232]. The restricted diffusivity of the solid of interest with a mean molecular radius r_{mol} in the extracellular matrix is calculated from the equation,

$$D_f = D \cdot \exp\left(-(1-\epsilon_f)^{1/2}\left(1 + \frac{r_{mol}}{r_f}\right)\right), \tag{7.18}$$

where D is the solute diffusivity in water and D_f is the restricted diffusion in the fiber matrix. According to [235] the hindrance coefficient for convective transport in the fibre matrix can be obtained from,

$$\gamma_f = 2 - \Phi_f. \tag{7.19}$$

The reduction coefficient Φ_f represents the relation between the space available to the solute relative to the space available to water,

$$\Phi_f = \exp\left[-(1-\epsilon_f)\left(\frac{2r_{mol}}{r_f} + \frac{r_{mol}^2}{r_f^2}\right)\right]$$

As discussed in Chapter 1, the media is formed by layers of smooth muscle cells. The presence of such cells is also observed in the case of a thickened intima. The contribution of smooth muscle cells is included in the model by means of an additional volume fraction ϵ_{SMC} that reduces the total porosity of the wall layer $\epsilon_{eff} = \epsilon_f(1-\epsilon_{SMC})$. In this case the transport parameters (diffusivity, Darcy permeability and lag coefficient) have to be transformed into effective parameters, see [235]. Without smooth muscle cells the parameters calculated from the equations (7.17)–(7.19) represent the effective parameters.

Example 7.2.1 (Intima) The mean radius of the fibres building up the extracellular matrix of the intima is $r_f = 3.22\,\mathrm{nm}$ [235]. By assuming an average spacing of 5 nm and an average ratio between fibre length and intima thickness of 1.5 [232] we get a total length of the fibres within the unit volume of $l_f = 1.225 \cdot 10 - 3\,\mathrm{nm}^{-2}$ and therewith a fractional void volume of $\epsilon_f = 0.96$ and a Darcy permeability of $K_{D,f} = 8.7 \cdot 10^{-13}\,\mathrm{cm2/(s \cdot dyne)}$. For LDL with a mean molecule radius $r_{mol} = 11\,\mathrm{nm}$ we get a restricted diffusivity of $D_f = 1.2 \cdot 10^{-7}\,\mathrm{cm2/s}$ and a reduction coefficient of $\Phi_f = 0.47$.

Example 7.2.2 (Media) The fractional void volume of the fibres in the media is $\epsilon_f = 0.43$ and the fraction of the smooth muscle cells is $\epsilon_{SMC} = 0.4$ which results in an effective values of $\epsilon_{eff} = 0.258$, $K_{D,eff} = 7.75 \cdot 10^{-16}\,\mathrm{cm2/(s \cdot dyne)}$, $\Phi_{eff} = 6.8 \cdot 10^{-6}$, $D_{eff} = 8.14 \cdot 10^{-9}\,\mathrm{cm2/s}$.

Transport across the endothelium and internal elastic lamina

The endothelium and the internal elastic lamina (IEL) are treated as selective permeable membranes. They are assumed to be layers of constant thickness H. Exchange of water and solutes across the endothelium takes place through clefts (pores) which occur between the endothelial cells. The pores can be divided into normal endothelial clefts which are modelled as cylindrical pores and leaky junctions which are approximated as pores with a ringlike cross-section surrounding the leaky cells (cells which are either dying or in mitosis). The IEL contains fenestral pores through which transport between the intima and the media takes place. According to [232] the fenestrae can be approximated as cylindrical pores. The transport of molecules which is small in relation to the pore size across such porous membranes can be basically described using the convection-diffusion-reaction equation. The only effect of the porous membrane on the transport is the reduction of the space available to the solution. The transport of large molecules through these membranes is highly restricted by the pore structure. It is assumed that for entrance into the pore a molecule must pass through the opening without striking the edge [270]. This restriction causes the reflection and sieving of large molecules at the surface of membranes with relatively small pores. During the transport through the pores the molecules collide with the pore walls. These interactions between the molecules and the pore walls causes a loss in the kinetic energy of the molecules which results in a restricted transport within the pores.

We subdivide the pores on the endothelium and IEL into cylindrical pores and pores with ring-like cross section. The hydraulic conductivity of a cylindrical pore is,

$$L_p = \frac{\rho_{pore}\pi R^4}{8\mu L},$$

where ρ_{pore} is the average density of the pores, R is the radius and L the length of the pore. The restricted diffusivity coefficient in the pore D_p is defined as

$$D_p = DF(\alpha),$$

where $\alpha = r_{mol}/R$ is the ratio between the molecule radius and the radius of the pores and $F(\alpha)$ is, from [106],

$$F(\alpha) = \left[2(1-\alpha)^2 - (1-\alpha)^4\right]\left[1 - 2.1\alpha + 2.09\alpha^3 - 0.95\alpha^5\right].$$

Then, the permeability of the pore can be calculated by

$$\mathcal{P}_p = \Phi D_p/L, \tag{7.20}$$

where $\Phi = (1-\alpha)^2$ considers the reduction of pore cross section that is available to the solute. Fig. 7.2 (left) shows the relation of the free and the restricted pore diffusivity as function of α. The osmotic reflection coefficient is calculated by following the equation, which is obtained in [11],

$$\sigma_{d,p} = (1-\Phi)^2$$

and the solvent drag reflection coefficient is given according to [106] by,

$$\sigma_{f,p} = \frac{16}{3}\alpha^2 - \frac{20}{3}\alpha^3 + \frac{7}{3}\alpha^4.$$

The functions the reflection coefficients are depicted in Fig. 7.2 (right).

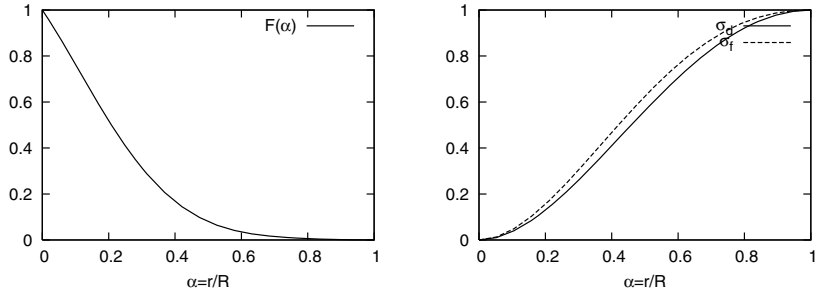

Fig. 7.2. Relation between the pore diffusivity and the free diffusivity (left), the osmotic reflection coefficient and the solvent drag reflection coefficient (right) as functions of the relation between the molecule and the pore radius, α

A pore with a ringlike cross-section is treated in the same way like a infinite long slit with constant width $2b$ as proposed by [106]. Hence the hydraulic conductivity of a ringlike pore is given by,

$$L_s = \frac{b^2}{3\mu L}. \tag{7.21}$$

The restricted diffusivity coefficient in the pore D_s is defined as,

$$D_s = DF_s(\alpha_s),$$

where $\alpha_s = r_{mol}/b$ is the ratio of the molecule radius to the half pore width size. The function of the restricted pore diffusivity [105] is,

$$F_s(\alpha_s) = (1-\alpha_s)\left(1 - 1.004\alpha_s + 0.418\alpha_s^3 - 0.169\alpha_s^5\right).$$

The permeability of the pore is calculated in the same way like the circular pore (7.20), where $\Phi_s = 1-\alpha_s$ accounts for the reduction of pore cross section that is available to the solute. The osmotic reflection coefficient follows form the model of [11],

$$\sigma_{d,s} = (1-\Phi_s)^2 = \alpha_s^2$$

and the solvent drag coefficient [105] equals to

$$\sigma_{f,s} = 1 - \left(1 - \frac{3}{2}\alpha_s^2 + \frac{1}{2}\alpha_s^3\right)\left(1 - \frac{1}{3}\alpha_s^2\right).$$

The functions the reflection coefficients are depicted in Fig. 7.3.

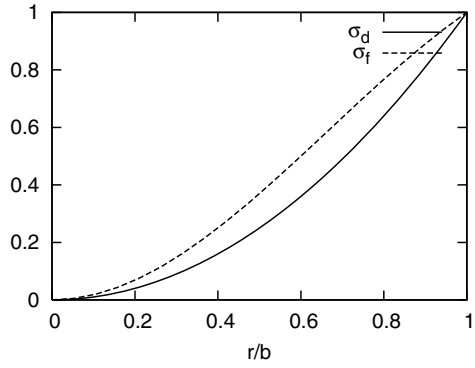

Fig. 7.3. Osmotic reflection coefficient and solvent drag reflection coefficient as functions of the ratio between molecule and half width size of the pore

Example 7.2.3 (Endothelium) The transport parameters of the leaky clefts ($L_{p,lj}$, $\mathcal{P}_{lj}$, Φ_{lj}, $\sigma_{f,lj}$, $\sigma_{d,lj}$) and the normal junctions($L_{p,nj}$, $\mathcal{P}_{nj}$, $\sigma_{f,nj}$, $\sigma_{d,nj}$) are calculated by equations described above. According to [232], the values of the hydraulic conductivity, permeability and reflection coefficients of the endothelium containing normal clefts and leaky clefts are

$$L_{p,end} = L_{p,nj} + L_{p,lj}\epsilon_{lj}$$

$$\mathcal{P}_{end} = \mathcal{P}_{nj} + \mathcal{P}_{lj}\epsilon_{lj}\Phi_{lj}$$

$$\sigma = \frac{L_{p,nj}\sigma_{nj} + L_{p,lj}\epsilon_{lj}\sigma_{lj}}{L_{p,e}},$$

where ϵ_{lj} is the area of leaky clefts per unit area of the endothelial surface. The average fraction of leaky cells for a healthy endothelium is 0.05 %. Their cell radius is 15 µm and the width is 20 nm–25 nm. The normal junctions have a radius of 5.5 nm and an average distance of 2.5 µm [232]. The resulting hydraulic conductivity is $L_{p,end} = 3 \cdot 10^{-11}\,\mathrm{cm3/(s \cdot dyne)}$. For LDL the permeability is $\mathcal{P}_{end} = 1.07 \cdot 10^{-11}\,\mathrm{cm/s}$ and the reflection coefficients are $\sigma_{d,end} = 0.996$ and $\sigma_{f,end} = 0.997$.

Example 7.2.4 (Internal elastic lamina) The average radius of the fenestral pores of the IEL is 0.15 µm [278] and their average density is $2210/mm2$ [235].The resulting hydraulic conductivity is $L_{p,IEL} = 3.05{\cdot}10^{-9}\,\mathrm{cm3/(s \cdot dyne)}$. For LDL the permeability is $\mathcal{P}_{IEL} = 1.59 \cdot 10^{-7}\,\mathrm{cm/s}$ and the reflection coefficients are $\sigma_{d,IEL} = 1.99 \cdot 10^{-2}$ and $\sigma_{f,IEL} = 1.93 \cdot 10^{-2}$.

7.2.2 Electrical analogy

Although the idea of applying an electrical analogy to set up reduced models for transport phenomena, including fluid flows, will be introduced in Chapter 10, we address here for the first time its application to mass transfer, more precisely to convection and diffusion processes.

The models to calculate the transport parameters described in the previous section are based on the assumption that the transport of the considered molecules occurs only in the fluid phase of the different layers. The transcellular transport, representing an essential part of the complete solid dynamics for very large molecules [355], cannot be considered in this kind of models. Therefore the help of experimental measurements is needed to make the theoretical estimations successful in the specific applications.

In this section a short overview of a methodology is presented that allows to estimate the physical parameters of the wall layers starting from a set of data that can be easily determined by experimental measurements like LDL concentration profiles in the arterial wall (see [49, 129, 326, 492]). A simplified problem is used to define the relationship between the set of physical parameters characterizing the wall (formally denoted with the vector $\mathbf{p}$) and

the concentration profiles of LDL the wall (described as a collection of concentration samples stored in the vector $\mathbf{c}$). The mathematical relationship between $\mathbf{p}$ and $\mathbf{c}$ will be denoted with $\mathbf{c} = F(\mathbf{p})$. We search for an analytical expression of F, which could be easily inverted leading to an explicit solution of the inverse problem $\mathbf{p} = F^{-1}(\mathbf{c})$. For this reason, an electrical analogy is applied to describe the mass transfer phenomena through the arterial walls. The derivation of the electrical analogy and its application to the transport through the wall layers is described in detail in [397].

Fluid dynamics

The electrical analog of the arterial wall with respect to fluid dynamics can be represented as a sequence of four resistances in series, corresponding to each single layer constituting the wall, as shown in Fig. 7.4.

The electrical representation of each layer is derived by a simplification of the governing equations for the fluid dynamics (first Kedem-Katchalsky equation and Darcy's law). The pressure drop is the driving force resulting in a volume flux representing the flux of the electrical analogy.

Using the transport parameters obtained from pore theory results in a filtration velocity of $J_v = 4.25 \cdot 10^{-7}\,\mathrm{cm/s}$ by applying a pressure drop of 70 mmHg. This value does not correspond to the measurements reported in [326]. Therefore the electric analog is used to rescale the parameters from pore theory to obtain the measured flux of $J_v = \boldsymbol{u} \cdot \boldsymbol{n} = 1.78 \cdot 10^{-6}\,\mathrm{cm/s}$. The updated transport parameters for the fluid dynamics are $L_{p,end} = 1.20 \cdot 10^{-10}\,\mathrm{cm^3/(s \cdot dyne)}$, $K_{D,i} = 3.64 \cdot 10^{-12}\,\mathrm{cm^2/(s \cdot dyne)}$, $L_{p,IEL} = 1.28 \cdot 10^{-8}\,\mathrm{cm^3/(s \cdot dyne)}$ and $K_{D,m} = 3.24 \cdot 10^{15}\,\mathrm{cm^3/(s \cdot dyne)}$.

Dynamics of chemicals

The simplification of the equations describing the solid dynamics in membranes and porous media (second Kedem-Katchalsky and advection-diffusion-reaction equation) ends up with an electrical analogy of two parallel resistances for each layer. These resistances represent the convective and the diffusive solid transport.

The electrical analog of the system featuring the different wall layers with respect to the transfer of molecules is represented in Fig. 7.5. The first two

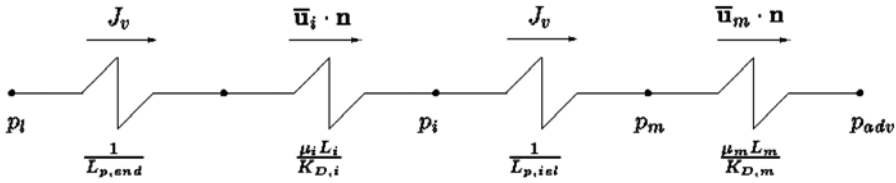

Fig. 7.4. Electrical analog-on for the plasma filtration inside the arterial wall

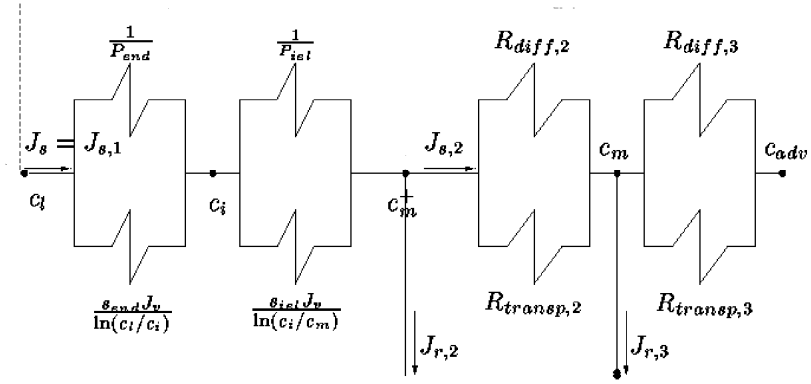

Fig. 7.5. Electrical analogon for the dynamics of chemicals of the arterial wall

modules represent the endothelium and the IEL, the remaining ones represent the media. Since the media is the thickest layer it is split in two parts, as this makes easier to take into account of the degradation of solute due to chemical reactions. Furthermore, physical experience suggests that the intima is the less resistant layer to diffusion transport. Consequently, to simplify our model, it is assumed that the concentration drop across the intima is negligible.

By fixing the value of the parameters that are experimentally determined with reasonable accuracy, precisely the wall thickness $L = 200\,\mu\text{m}$, the solute diffusivity inside the media, $D_m = 8 \cdot 10^{-9}$, and the porosity of the media, $\epsilon_m = 0.15$ we are able to cacluate the missing set of parameters starting from a number of experimentally measured concentration values. For instance we consider $\bar{c}_m^+ = 10^{-2}, \bar{c}_m = 2.5 \cdot 10^{-3}, \bar{c}_m^- = 10^{-2}$, given by [326]. The concentration in the intima is considered as unknown that will be determined by means of the equation arising from the electrical analogy. A detailed description of the complete procedure can be found in [397]. As a result of that, we determine the missing set of transport parameters that are given by $\mathcal{P}_{end} = 2 \cdot 10^{-8}\,\text{cm/s}$, $\mathcal{P}_{IEL} = 3.18 \cdot 10^{-4}\,\text{cm/s}$, $\sigma_{end} = 0.998$, $\sigma_{IEL} = 0.983$, $\gamma_i = 0.17$, $\gamma_m = 0.117$ and $r_m = 3.197 \cdot 10^{-4}\,\text{s}^{-1}$.

7.3 Computer simulation

This section is devoted to the numerical approximation of the mathematical models which have been introduced in Section 7.1. First of all, we point out that a self contained treatment of the topics involved in the numerical approximation of partial differential equations would be rather extensive and complex, and consequently it goes beyond the scope of this chapter and of this book. For this reason, the aim of this section is to provide a survey on numerical approximation of PDEs and computational fluid dynamics that is specifically adapted to the problems involved on the mass transfer in the car-

diovascular system. We will enter into details only for those topics that are peculiar to this matter. Furthermore, we will provide at first an overview and the main references to build up the numercal discretisation of the multilayer model. Then, we will consider a simplified model where the arterial walls are assumed to be an homogeneous layer. In this context, we will address those topics that are peculiar to the treatment of mass transfer in the arterial walls.

As already seen, the multilayer model involves the coupling of the flow equations for blood and plasma, with an advection-diffusion-reaction problem (see Problems 7.1.1 and 7.1.2 respectively). In these models, the advection-diffusion-reaction equations depend on the fluid dynamics through the advective field. Hence the fluid dynamics problem is solved at a first step, and then we solve the advection-diffusion-reaction problem.

For the space discretisation of the space-dependent partial differential operators, we apply the finite element method. In particular, for what concerns the Navier–Stokes equations, in order to satisfy the compatibility *inf-sup* condition, we have adopted a linear approximation based on the so-called $\mathbb{P}^1 iso \mathbb{P}^2 - \mathbb{P}^1$ element, while the backward Euler time discretisation has been coupled with a semi-implicit treatment of the nonlinear term. Finally, a splitting of the velocity and pressure problem based on the so-called *Yosida method* is carried out. For more details about these techniques, the interested reader is referred to [404, 405, 407].

For the discretisation of the Darcy problem we consider a mixed-hybrid finite element formulation based on Raviart-Thomas elements, for which we refer to [79]. By means of this method we approximate $\boldsymbol{u}_i, p_i$ and $\boldsymbol{u}_m, p_m$ by means of $\mathbb{RT}^0 - \mathbb{P}^0$ elements. Then, the discrete velocities are projected by means of the standard L^2 inner product on the space of vector valued linear finite elements in order to be more easily exploited in the discretisation of the solute dynamics problem.

Concerning the advection-diffusion equations, we observe that the multilayer problem is characterised by very low diffusivity coefficients. In other terms, this problem is dominated by the advection effects. Indeed, if h denotes the space discretisation step (which in our simulations is in the range of 10^{-2}cm), $|\boldsymbol{u}|$ is a representative value of the blood velocity, for instance equal to 10cm/s, and the diffusivity of LDL is about $D = 10^{-7}\text{cm}^2/\text{s}$, we have an indicative value of the *local Péclet number*, $Pe = h|\boldsymbol{u}|D^{-1}$, (which weighs the convection effects with respect to the diffusive ones) of 10^6. As it is well known, finite element techniques (and in general Galerkin methods) could be inaccurate when facing convection dominated problems and resorting to a stabilisation technique becomes mandatory. Different strategies can be pursued in this regard: the interested reader is referred to [236] and [407]. In our simulations, streamline-upwind/Petrov–Galerkin (SUPG) has been successfully adopted and will be addressed later on.

A further difficulty is related to the fact that we consider phenomena that take place both into blood and into the arterial tissues. By consequence, from the point of view of either fluid dynamics or solute dynamics, we notice that

the multilayer problem, as well as its simplified variants, can not be reformulated as problems governed by a unique differential operator on a single domain. For this reason, we focus our attention on *iterative substructuring methods* to split the multilayer problem into subproblems. For the treatment of this topic, we will focus on the solute dynamics model, namely Problem 7.1.2, which consists mainly in a system of advection-diffusion equations on adjacent domains coupled by suitable matching conditions. A general theory, discussed for instance by Quarteroni and Valli in [408], is available for this matter in the case of linear symmetric problems, for example diffusion dominated processes, but the presence of a non negligible advection term makes the multilayer problem to be governed by strongly unsymmetric operators. Furthermore, the specific matching conditions that we apply between blood and the arterial walls are definitely non-standard and in particular they are nonlinear. Consequently, the general framework of [408] does not apply to our case. Thus, in this section we will discuss in detail the convergence properties of the iterative substructuring methods suitable for the multilayer problem.

7.3.1 Numerical approximation of the solute dynamics

As already mentioned, in order to concentrate on the main ideas and to simplify at most the notation and the technical aspects of this subject, we do not consider here the complete multilayer problem 7.1.2. Instead of the multilayer model we consider an instance of the fluid-wall models, where the complex heterogeneous structure of the arterial walls is approximated by a simple homogeneous layer. Such model, proposed in [137, 138] to study the concentration of oxygen and LDL within the arterial walls, reads as follows:

Problem 7.3.1 Find the concentrations c_l, defined on $\Omega_l \times [0,T]$, and c_w, defined on $\Omega_w \times [0,T]$, such that

$$\begin{aligned}
&\frac{\partial c_l}{\partial t} + \mathbf{div}(-D_l \boldsymbol{\nabla} c_l + \boldsymbol{u}_l c_l) = f_l, \quad \text{in } \Omega_l,\ t>0 \\
&c_l = c_{l,in} \quad \text{on } \Gamma_{l,in},\ t>0 \\
&D_l \boldsymbol{\nabla} c_l \cdot \boldsymbol{n}_l = 0 \quad \text{on } \Gamma_{l,out}, \quad t>0 \\
&c_l(0) = c_{l,0} \quad \text{in } \Omega_l, \quad t=0,
\end{aligned} \tag{7.22}$$

$$\begin{aligned}
&\frac{\partial c_w}{\partial t} - \mathbf{div}(D_w \boldsymbol{\nabla} c_w) = f_w \quad \text{in } \Omega_w, \quad t>0 \\
&c_w = c_{w,ext} \quad \text{on } \Gamma_{w,ext}, \quad t>0 \\
&D_w \boldsymbol{\nabla} c_w \cdot \boldsymbol{n}_w = 0, \quad \text{on } \Gamma_{w,in} \cup \Gamma_{w,out},\ t>0, \\
&c_w(0) = c_{w,0} \quad \text{in } \Omega_w,\ t=0,
\end{aligned} \tag{7.23}$$

with the following matching conditions at the interface,

$$D_w \boldsymbol{\nabla} c_w \cdot \boldsymbol{n}_w = -D_l \boldsymbol{\nabla} c_l \cdot \boldsymbol{n}_l \quad \text{on } \Gamma, \quad t > 0, \tag{7.24}$$

$$-D_l \boldsymbol{\nabla} c_l \cdot \boldsymbol{n}_l = \mathcal{P}(c_l - c_w) \quad \text{on } \Gamma, \quad t > 0, \tag{7.25}$$

where the notation of Section 7.1 has been mantained.

In order to define the numerical discretisation of Problem 7.3.1 we introduce $\mathcal{T}_{h,l}, \mathcal{T}_{h,w}$ admissible triangulations of $\overline{\Omega}_l, \overline{\Omega}_w$ respectively. Moreover, we assume that $\mathcal{T}_{h,l}, \mathcal{T}_{h,w}$ are conforming triangulations on Γ. In other words we require that $\mathcal{T}_h = \mathcal{T}_{h,l} \cup \mathcal{T}_{h,w}$ is an admissible triangulation for $\overline{\Omega}_l \cup \overline{\Omega}_w$. Then, we are in position to define the finite element spaces,

$$\begin{aligned} V_{h,l} =& \{v_{h,l} \in C^0(\overline{\Omega}_l) \mid v_{h,l} \in \mathbb{P}_k, \ \forall K \in \mathcal{T}_{h,l}, \ v_{h,l}|_{\Gamma_{l,in}} = 0\} \\ V_{h,w} =& \{v_{h,w} \in C^0(\overline{\Omega}_w) \mid v_{h,w} \in \mathbb{P}_k, \ \forall K \in \mathcal{T}_{h,w}, \ v_{h,w}|_{\Gamma_{w,ext}}, \ v_{h,m}|_{\Gamma_{adv}} = 0\}. \end{aligned}$$

Moreover, let Λ_h be the finite dimensional space defined by the traces on Γ of functions in $V_{h,l}$ or $V_{h,w}$. To introduce the time discretisation we subdivide the time interval $[0, T]$ in N time steps $t^n = n\Delta t$ with $\Delta t > 0$ and $n = 1, \ldots, N$, and use backward Euler finite difference schemes. In order to simplify our notation, let us introduce the following time discrete bilinear forms,

$$a_l^n(w, v) = \frac{1}{\Delta t}(w, v) + (D_l \boldsymbol{\nabla} w, \boldsymbol{\nabla} v) + \left(\boldsymbol{u}_{h,l}^n \cdot \boldsymbol{\nabla} w, v\right), \tag{7.26}$$

$$a_w^n(w, v) = \frac{1}{\Delta t}(w, v) + (D_w \boldsymbol{\nabla} w, \boldsymbol{\nabla} v), \tag{7.27}$$

and the corresponding right hand side terms, $\mathcal{F}_\lambda^{n-1} = f_\lambda + \frac{1}{\Delta t} c_\lambda^{n-1}$ for $\lambda = l, w$. The fully discrete counterpart of the fluid-wall model reads as follows:

Problem 7.3.2 For all $n = 1, \ldots, N$, given $[c_{h,l}^0, c_{h,w}^0] \in V_{h,l} \times V_{h,w}$, find $c_{h,l}^n \in V_l, c_{h,w}^n \in V_{h,w}$ such that

$$\begin{aligned} a_l^n\left(c_{h,l}^n, v_{h,l}\right) + \left(c_{h,l}^n, v_{h,l}\right)_{\mathcal{P}} &= \left(c_{h,w}^n, v_{h,l}\right)_{\mathcal{P}} + \left(\mathcal{F}_l^{n-1}, v_{h,l}\right) \quad \forall v_{h,l} \in V_{h,l} \\ a_w^n\left(c_{h,w}^n, v_{h,w}\right) + \left(c_{h,w}^n, v_{h,w}\right)_{\mathcal{P}} &= \left(c_{h,l}^n, v_{h,w}\right)_{\mathcal{P}} + \left(\mathcal{F}_w^{n-1}, v_{h,w}\right) \quad \forall v_{h,w} \in V_{h,w}. \end{aligned} \tag{7.28}$$

Let us now introduce the algebraic counterpart of Problem 7.3.2. To this aim, let us denote with $\mathbf{c}_\lambda^n \in \mathbb{R}^{N_\lambda}, \lambda = l, w$ the vectors of the degrees of freedom of the discrete approximation of the concentration on $\mathcal{T}_{h,\lambda}$. The application of Lagrangian finite elements leads to systems of algebraic equations for the unknowns $\mathbf{c}_\lambda^n$. More precisely, at every time step t^n, Problem 7.3.2 leads to the system of linear equations,

$$A^n \mathbf{c}^n = \mathbf{b}^n \quad \Leftrightarrow \quad \begin{bmatrix} A_{ll}^n & A_{lw}^n \\ A_{wl}^n & A_{ww}^n \end{bmatrix} \cdot \begin{bmatrix} \mathbf{c}_l^n \\ \mathbf{c}_w^n \end{bmatrix} = \begin{bmatrix} \mathbf{b}_l^n \\ \mathbf{b}_w^n \end{bmatrix} \tag{7.29}$$

Denoting with $\{\psi_{i,l}\}, i = 1, \ldots, N_l$ and $\{\psi_{i,w}\}, i = 1, \ldots, N_w$ the set of linear finite element shape functions of $V_{h,l}, V_{h,w}$ respectively, the matrices $A^n_{ll}, A^n_{lw}, A^n_{wl}, A^n_{ww}$ are defined as follows.

$$
\begin{aligned}
[A^n_{ll}]_{i,j} &= a^n_l(\psi_{j,l}, \psi_{i,l}) + (\psi_{j,l}, \psi_{i,l})_{\mathcal{P}} \quad i = 1, \ldots, N_l,\ j = 1, \ldots, N_l,\\
[A^n_{lw}]_{i,j} &= -(\psi_{j,w}, \psi_{i,l})_{\mathcal{P}} \quad i = 1, \ldots, N_l,\ j = 1, \ldots, N_w,\\
[A^n_{wl}]_{i,j} &= -(\psi_{j,l}, \psi_{i,w})_{\mathcal{P}} \quad i = 1, \ldots, N_w,\ j = 1, \ldots, N_l,\\
[A^n_{ww}]_{i,j} &= a^n_w(\psi_{j,w}, \psi_{i,w}) + (\psi_{j,w}, \psi_{i,w})_{\mathcal{P}} \quad i = 1, \ldots, N_w,\ j = 1, \ldots, N_w.
\end{aligned}
$$

Moreover, the right hand sides $\mathbf{b}^n_l, \mathbf{b}^n_w$ are given by, $[\mathbf{b}^n_\lambda]_i = \left(\mathcal{F}^{n-1}_\lambda, \psi_{\lambda,i}\right)$ with $i = 1, \ldots, N_\lambda,\ \lambda = l, w$. The obvious strategy to solve system (7.29) consists of applying either direct or iterative methods to the global problem $A^n\mathbf{c}^n = \mathbf{b}^n$. An approach more specific to our case consists of splitting (7.29) into subsystems associated to the finite element discretisation on $\mathcal{T}_{h,l}, \mathcal{T}_{h,w}$ separately. The latter strategy seems more attractive, because it makes easier to handle a discontinuous concentration across the interface. Indeed, in the finite element framework, the concentration on the nodes laying on Γ has two different values, one associated to the lumen and one to the wall. Moreover, as we will see later, the analysis of iterative techniques to split Problems 7.3.2, suggests the way to build efficient preconditioners for the global system $A^n\mathbf{c}^n = \mathbf{b}^n$. The splitting technique gives even more advantages in the nonlinear case. In fact, an explicit treatment of the nonlinear term, allows us to reduce the solution of the multilayer problem to a sequence of linear subproblems.

7.3.2 Iterative substructuring methods for the solute dynamics

Since all the relevant equations deal only with unknowns evaluated at the time step t^n, for notational convenience from now on, we drop the index n. The time index will be explicitly indicated only when referring to a time step different than t^n. Moreover, since the results presented in this section hold true also in the infinite dimensional case with respect to space dependence, we drop the index h denoting the space discrete functions.

To split Problem 7.3.2 into subproblems, we introduce an iterative procedure where the concentration at the wall, in the advection diffusion equation in the lumen, is evaluated at the previous iterative step. This leads to the following iterative procedure:

$$
\begin{aligned}
&\tfrac{1}{\Delta t} c^k_l + \mathbf{div}(-D_l \boldsymbol{\nabla} c^k_l + \boldsymbol{u}_l c^k_l) = f_l + \tfrac{1}{\Delta t} c^{n-1}_l \quad \text{in } \Omega_l,\\
&c^k_l = c_{D,l}, \quad \text{on } \Gamma_{D,l},\\
&\boldsymbol{\nabla} c^k_l \cdot \boldsymbol{n}_l = 0 \text{ on } \Gamma_{N,l},\\
&-D_l \boldsymbol{\nabla} c^k_l \cdot \boldsymbol{n}_l = \mathcal{P}(c^k_l - c^{k-1}_w), \quad \text{on } \Gamma,
\end{aligned}
$$

$$\frac{1}{\Delta t}c_w^k + \mathbf{div}(-D_w \boldsymbol{\nabla} c_w^k + \boldsymbol{u}_w c_w^k) = f_w + \frac{1}{\Delta t}c_w^{n-1} \text{ in } \Omega_w,$$
$$c_w^k = c_{D,w}, \quad \text{on } \Gamma_{D,w},$$
$$\boldsymbol{\nabla} c_w^k \cdot \boldsymbol{n}_w = 0 \text{ on } \Gamma_{N,w},$$
$$-D_w \boldsymbol{\nabla} c_w^k \cdot \boldsymbol{n}_w = \mathcal{P}(c_w^k - c_l^k), \quad \text{on } \Gamma.$$

Reinterpreting this iterative method in the variational form, we obtain the following problem.

Problem 7.3.3 For all $n = 1, \ldots, N$, given an initial guess c_w^0 and a tolerance ϵ, for $k = 1, 2, \ldots$ find a sequence $[c_l^k, c_w^k]$ such that,

$$\begin{aligned} a_l^n\left(c_l^k, v_l\right) + \left(c_l^k, v_l\right)_{\mathcal{P}} &= \langle \mathcal{F}_l^{n-1}, v_l\rangle + \left(c_w^{k-1}, v_l\right)_{\mathcal{P}} \quad \forall v_l \in V_l \\ a_w^n\left(c_w^k, v_w\right) + \left(c_w^k, v_w\right)_{\mathcal{P}} &= \langle \mathcal{F}_w^{n-1}, v_w\rangle + \left(c_l^k, v_w\right)_{\mathcal{P}} \quad \forall v_w \in V_w, \end{aligned} \tag{7.30}$$

until the stopping criterion,

$$\frac{\|c_l^k - c_l^{k-1}\|_0}{\|c_l^k\|_0} + \frac{\|c_w^k - c_w^{k-1}\|_0}{\|c_w^k\|_0} < \epsilon \tag{7.31}$$

is satisfied.

Of course the stopping criterion can be modified. Such method is often referred as *Robin-Robin* iterative method, because the interaction between the subdomains is achieved by Robin matching conditions.

At this stage, the issue of major importance is to understand whether the iterative method presented in Problem 7.3.3 is convergent, or in other words to prove that the sequence $[c_l^k, c_w^k]$ converges in a suitable norm to the solution of Problem 7.3.2. Because of the lack of continuity between c_l and c_w at the interface Γ, the analysis of convergence for this splitting method does not straightforwardly follows from available convergence results, namely the Dirichlet-Neumann, the Neumann-Neumann or the Robin-Robin methods arising from domain decomposition techniques, for which we refer to [408]. We need thus to develop a specific analysis. First of all we introduce the *splitting error*, namely

$$e_{h,l}^{n,k} = c_{h,l}^n - c_{h,l}^{n,k}, \quad e_{h,w}^{n,k} = c_{h,w}^n - c_{h,w}^{n,k}$$

where $[c_{h,l}^n, c_{h,w}^n]$ is the solution of problem 7.3.2. As stated before, in the sequel we will use the abridged notation e_l^k, e_w^k. Now, if we subtract equations (7.30) from (7.28), we obtain the following equations for $[e_l^k, e_w^k]$, that we call the splitting error equations,

$$a_l^n\left(e_l^k, v_l\right) + \left(e_l^k, v_l\right)_{\mathcal{P}} = \left(e_w^{k-1}, v_l\right)_{\mathcal{P}} \quad \forall v_l \in V_l \tag{7.32}$$
$$a_w^n\left(e_w^k, v_w\right) + \left(e_w^k, v_w\right)_{\mathcal{P}} = \left(e_l^k, v_w\right)_{\mathcal{P}} \quad \forall v_w \in V_w. \tag{7.33}$$

We resume the convergence property of Problem 7.3.3 in the theorem below.

Property 7.3.1 *The iterative method defined in problem 7.3.3 is convergent (for both the Galerkin and the stabilised SUPG or GaLS discretisations). More precisely we have* $\lim_{k\to\infty} \|e_l^k\|_1 + \|e_w^k\|_1 = 0$. *The convergence rate may depend on the physical data but not on the mesh size* h.

Remark 7.3.1 (Advanced topics) *In the framework of the mathematical analysis of iterative substructuring methods, a more advanced approach consists in rewriting the the fluid-wall problem for an unknown living on the interface between the lumen and the wall. In this case, special Steklov-Poincaré operators, see [408] and [410], are necessary to consider the non standard Robin-Robin matching conditions. This reinterpretation leads to a detailed characterisation of the convergence properties of the iterative scheme of Problem 7.3.3, where a parameter that accelerates the convergence is introduced. This study, which is addressed in detail in [410], also suggests that the scheme of Problem 7.3.3 can be seen as an* optimal *preconditioner for the original coupled Problem 7.3.2. This observation give rise to the discussion of efficient computational techniques to solve the fluid-wall problem. In particular, the application of the* flexible preconditioned GMRES *method, proposed by Saad in [439] leads to a very efficient numerical scheme for the problems at hand.*

Furthermore, the introduction of mesh adaptive techniques would be an extremely useful goal useful goal to approximate accurately the mass transfer from the blood to the arterial walls. Some preliminary applications of anisotropic mesh adaptivity techniques to these problems have been presented in [161].

7.4 Numerical results and discussion

In this section we apply the models and methods developped so far to two study cases. To this aim we apply a common paradigm. First of all we introduce the geometrical model and then we discuss the lumeanl and transmural transport processes. In the first study we will analyse the effect of disturbed flow patterns (flow separation, stagnation and recirculation) inside an axisymetric stenosed artery, while in the second case we consider a realistic 3D bifurcation. These results are discussed with further details in [395].

In the case of the stenosed axisymetric arterial segment we will focus our attention on the influence of local flow recirculation and separation downstream the stenosis on the LDL transport. Additionally the impact of the different wall models (fluid-wall model and multilayer model) on the concentration distribution inside the wall will be addressed. Due to the low diffusivity of the substances of interest (LDL) the lumenal transport is highly convection dominated and therefore strongly influenced by the flow patterns. The water-permeable nature of the arterial wall and the related transmural plasma filtration determine a local accumulation of LDL at the blood/wall interface.

In the case of the realistic human carotid bifurcation geometry only the fluid-wall model is applied to simulate the coupled lumenal and transmural

transport process. In this case the influence of the resulting complex inplane flow patterns on the LDL transport will be discussed.

In both cases the blood flow in the arterial lumen has a mean velocity of $U_0 = 15.7\,\mathrm{cm/s}$, the reference length (lumenal inflow diameter) is $L_0 = 0.67\,\mathrm{cm}$. Blood is modelled as Newtonian fluid with the apparent viscosity $\mu = 0.035$ Poise and the constant fluid density $\rho = 1.05\,\mathrm{g/cm^3}$ leading to a Reynolds number $Re = 300$. The viscosity of plasma in the arterial wall is $\mu_p = 0.7210^{-2}\,\mathrm{cm^2/s}$ and a constant pressure drop of $p_l - p_{adv} = 70\,\mathrm{mmHg}$ across the arterial wall is assumed. The studies only focus on the stationary flow because in the case of macromolecules (LDL) and constant transport parameters of the wall layers the influence of pulsatility on the LDL distribution is very small.

7.4.1 LDL transport in a stenosed axisymetric artery

Geometrical model

The influence of flow separation onto the LDL transport processes is analysed in a simplified geometrical model of an axisymetric stenosed arterial segment (Fig. 7.6). The computational domain has a total length of $70L_0$, where L_0 is the arterial diameter. The length of the stenotic region is $1.5L_0$. The upstream and downstream lengths with respect to the stenotic region are $18.75L_0$ and $49.75L_0$, respectively. The minimal section is equal to the 25 % of the inflow one. The thickness of the arterial wall in the fluid-wall model and of the media in the multilayer model is $200\,\mu\mathrm{m}$ ($0.03L_0$). The thickness of the intima in the multilayer wall case is $10\,\mu\mathrm{m}$ ($0.0015L_0$). The wall thickness is uniform along the artery.

The finite element meshes consist of 50082 velocity/pressure elements for the lumen, 14730 velocity/pressure elements for the wall (media) and additionally 4910 velocity/pressure elements for the discretisation of the intima in the multilayer model. For the calculation of the concentration field each velocity/pressure element was subdivided into 16 concentration elements resulting in 801312 elements in the lumen, 235680 elements in the wall (media) and 78560 concentration elements in the intima.

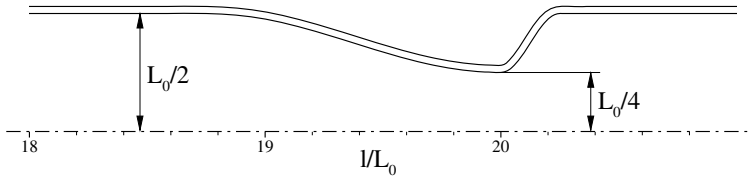

Fig. 7.6. Geometrical model of the stenosed tube

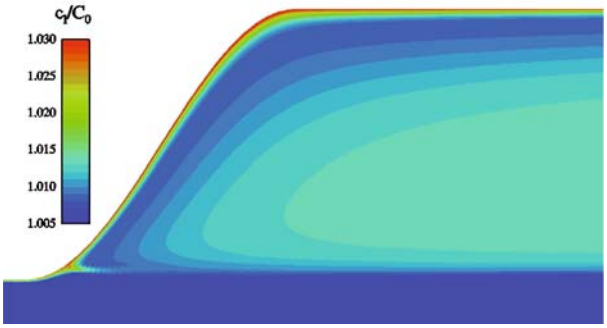

Fig. 7.7. Concentration contours near the stenosis

Lumenal LDL distribution

The development of lumenal surface concentration and the effect of flow separation on the local mass transfer to and into the wall in the downstream region of the stenosis is demonstrated in Fig. 7.7. The figure shows LDL accumulation near the tube wall. The equilibrium concentration at the fluid-endothelium boundary is higher than the concentration in the bulk stream. This polarisation effect at the surface occurs due to the plasma-permeability of the wall. The figure displays the steep concentration gradient across the separating streamline and a concentration increase of about one percent in the separation region compared to the bulk concentration. At the wall region directly downstream the stenosis a decrease of surface concentration polarisation can be observed.

The results of the mass transport study support the conclusion that the filtration process at the wall causes a lumenal surface concentration of LDL which is a dominant effect of mass transport processes including plasma-permeable walls. Flow separation downstream the axisymmetric stenosis influences the concentration boundary layer resulting in a decrease of surface concentration. The equilibrium concentration at the lumenal surface depends on the local convective transport near the surface in the lumen, on the filtration velocity of plasma into the wall and on the diffusive processes of the molecules.

Transmural transport processes

Fig. 7.8 shows the normal velocity contours in the media (panel a) and the velocity vectors in the media and in the intima (panel b) for the multilayer model in the expanding region. The magnitude of the normal velocity is uniform and mainly determined by the pressure gradient across the arterial wall. However, small but non negligible velocity gradients can be related to the geometrical shape of the arterial wall. More precisely, due to the convex curvature at $l/L_0 = 20$ we observe a decreasing cross-sectional area in radial direction. As a result of that, the wall velocity increases at the outer region of the arterial

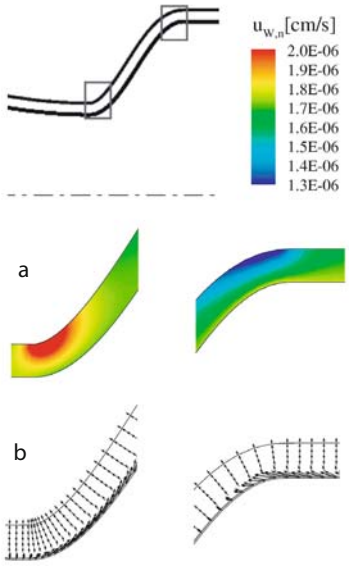

Fig. 7.8. Normal velocity contours in the media (panel a) and the velocity vectors in the media and in the intima (panel b) for the multilayer wall model in the expanding region

wall. On the other hand, because of the concave wall shape at $l/L_0 = 20.25$, the increasing cross-sectional area causes a decreasing wall velocity in radial direction. However, we observe that the normal velocity at the endothelium is only slightly affected by these geometrical properties and its value is about $J_v = 1.76 \cdot 10^{-6}$ cm/s in the expansion region, in very good agreement with the available measurements. The multilayer model also provides the flow field in the intima. The pressure drop across this layer is very low compared to the pressure drop across the whole arterial wall, while we observe high pressure gradients in the expanding region of the lumen. As a result of this, a high axial wall velocity occurs within the intima (Fig. 7.8 panel b). On the other hand, in the media the dominating driving force is the pressure gradient in the normal direction and consequently the axial flow is of minor importance.

These irregularities in the flow field across the arterial wall influence the concentration distribution within the wall. Figure 7.9 display the concentration contours in the wall of the two different wall models at selected locations in the expanding region of the stenosis. We observe that the perturbations in the velocity field in the intima and the media affect the concentrations as well. For example in the media, the concentration in the region of high filtration velocities is slightly higher than the average value, while it is lower than the average in correspondence of low filtration velocities. This is also clearly put into evidence by Fig. 7.10 that provides a quantitative comparison of the profiles of c_l, c_m^+, c_m and c_m^- plotted along the axial coordinate.

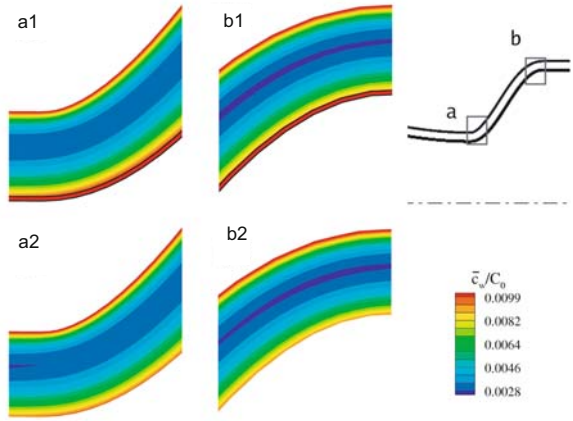

Fig. 7.9. Concentration contours provided by the fluid-wall model (bottom) and the multilayer model (top). In the latter case, the presence of the intima is put into evidence

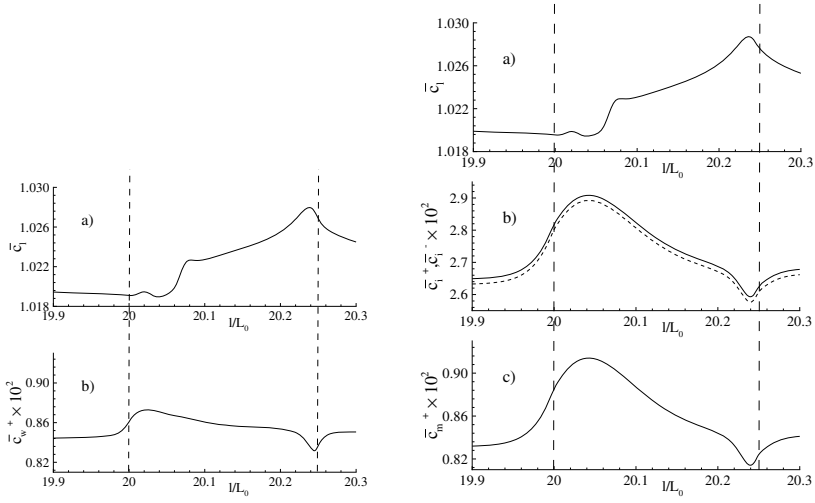

Fig. 7.10. Concentration values at the lumen-membrane boundary (panel a, left), the membrane-wall boundary (panel b, left) provided by the fluid-wall model. Concentration values at the lumen-endothelium boundary (panel a, right), the endothelium-intima boundary ((panel b, right), solid line), the intima-IEL boundary ((panel b, right), dashed line), the IEL-media boundary (panel c, right) computed with the multilayer model.

Focusing on Fig. 7.10 it can be seen that the lumenal concentration at the arterial wall is neither influenced by the concentration field in the arterial wall nor by the different wall models. The concentration polarisation mainly depends on the velocity field in the lumen. In particular, the polarisation effect is negligible where the blood flow is attached to the wall and the axial component is dominating. On the other hand, the filtration velocity normal to the wall surface sensibly influence the concentration field in the regions of blood recirculation where the axial flow next to the wall is highly reduced. Indeed, the maximal polarisation occurs at the expanding region of the stenosis where the recirculation zone has the largest extent (Fig. 7.10 panel a, left, and panel a, right). The behaviour of the wall concentration of the fluid-wall model (Fig 7.10 panel b, left) is qualitatively similar to the one observed with the multilayer model. However, the results provided by the two models differ from the quantitative point of view. We analyse the total variation of concentration reported for both the fluid-wall model and the multilayer model in Fig. 7.10 (on the left and on the right, respectively). We observe that for the fluid-wall model the increase in the concentration level due to the bending of the arterial wall results in about $0.26 \cdot 10^{-3}$ that corresponds to 3 % of the average concentration value on the membrane-wall interface. Conversely, for the multilayer model we obtain a similar profile but the increase in concentration in correspondence of the geometrical perturbation is equivalent to $0.8 \cdot 10^{-3}$, namely 9.5 % of the average concentration value. Consequently, we point out that the two models react very differently to the geometrical perturbation represented by the bending of the arterial wall. Indeed the ratio of the aforementioned figures is of order 3. The larger variations in the multilayer wall model can be explained by the additional presence of plasma filtration with high axial components in the intima, that can not be captured by the simpler fluid-wall model. In this examination the variations of concentration in the wall layers are within a few percent, but this values might change under different conditions (e.g. a damaged endothelium). Moreover, the peak in the multilayer case is located downstream with respect to the fluid-wall case. This could be explained by observing that in the multilayer model the axial velocity in the intima transports and accumulates molecules in the centre of the expansion region (identified by $20 < x/L_0 < 20.2$, see Fig. 7.8).

7.4.2 LDL transport in realistic model of a 3D carotid artery bifurcation

Geometrical model

An anatomically realistic computational model of a human carotid artery bifurcation has been developed by K. Perktold and his research group at the Graz University of Technology on the basis of an experimental lumenal cast prepared and digitalised by D. Liepsch, FH Munich, see [250, 379]. To develop the computational model surface measured surface data were smoothed using

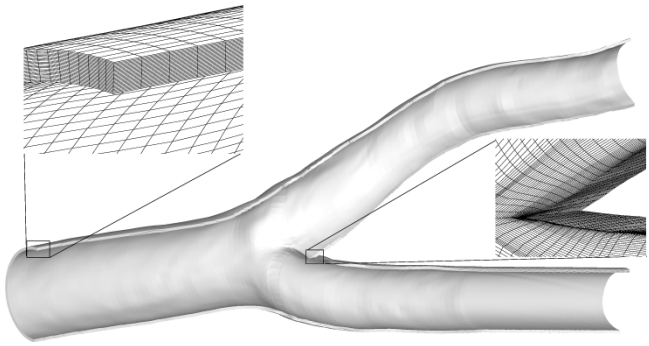

Fig. 7.11. Anatomically realistic computational model surface of the human carotid artery bifurcation

weighted least squares B-splines. This surface corresponds to the lumen/wall interface of the geometrical model. The arterial wall was created by the extension of the this surface in normal direction. A constant wall thickness of 200 µm (beside the region of the flow divider tip) was assumed (Fig. 7.11).

The finite element grid of the arterial lumen was generated applying a mesh generator based on local optimisation of geometric properties such as smoothness and orthogonality of the grid [380]. The finite element discretisation of the arterial wall was created by the extension of the lumenal grid at the lumen/wall surface in normal direction. The discretisation employs eight node isoparametric brick elements with tri-quadratic velocity and tri-linear pressure approximation. The subdivision yields 49 536 brick elements for the arterial lumen (resulting in 420 081 nodes for each velocity component and 55 601 nodes for the pressure) and 76 272 brick elements for the arterial wall (resulting in 656 265 nodes for each velocity component and 87 832 nodes for the pressure). For the solution of the mass transport problem each velocity element is subdivided into 32 subelements. The approximation of the transport problem applies tri-linear interpolation functions for the concentration resulting in 1 675 857 concentration nodes in the lumen and 2 537 587 concentration nodes in the arterial wall.

Lumenal transport processes

To illustrate the influence of the arterial geometry on the lumenal convective transport and the correlated LDL concentration distribution near the wall, Fig. 7.12 displays the wall shear stress and the concentration distribution at the interface lumen/membrane. The graphic demonstrates an accumulation of macromolecules at the lumen side of the membrane (Fig. 7.12 panel b). It is most pronounced in regions of low flow (indicated by low shear stress) occurring in the bifurcation region. At the flow divider walls of the bifurcation (high shear region) no accumulation of macromolecules occurs.

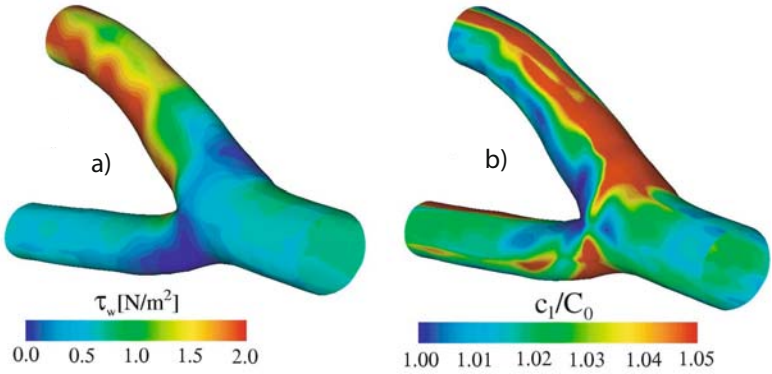

Fig. 7.12. Wall shear contours (panel a) and LDL concentration distribution (panel b) at the lumen-membrane interface

Fig. 7.13 displays the lumenal LDL concentration distribution and the inplane velocity component at different cross-sections in and downstream the bifurcation region. Downstream near the bifurcation (cross-section B), two symmetric vortices occur. This typical Dean flow is superposed further downstream by secondary motion caused by the nonplanarities of the vessel. It can be seen that at the sites of stagnating inplane motion at the outer wall of the vessel high polarisation occurs also downstream the bifurcation (level B,C and D). This points out a strong correlation between concentration polarisation and inplane motion. Indeed the inplane motion can be interpreted as additional convective effect which transports the accumulated macromolecules back to the bulk flow and reduces the polarisation of LDL near the arterial wall.

Transmural transport processes

The plasma flow field at the interface membrane/wall is shown in Fig. 7.14. Due to the high pressure gradient across the wall (70 mmHg) the velocity field vectors are mainly oriented in normal direction (Fig. 7.14 panel a). The low pressure drop along the vessel segment results in a small axial component of the plasma field in the range of 10^{-8} cm/s. This axial component is about 100 times lower than the average value of the filtration velocity in normal direction of 1.7610^{-6} cm/s. A 0.7 % variation of the filtration velocity occurs due to the non-constant pressure distribution at the lumenal side that results from the superposition of hydrostatic and hydrodynamic pressure (Fig. 7.14 panel b).

Figure 7.15 shows the concentration profile across the wall at selected points. The small variations of the plasma velocity field and the constant transport parameters of the wall layers result in a relatively uniform concentration distribution of LDL in the arterial wall. The typically U-shaped

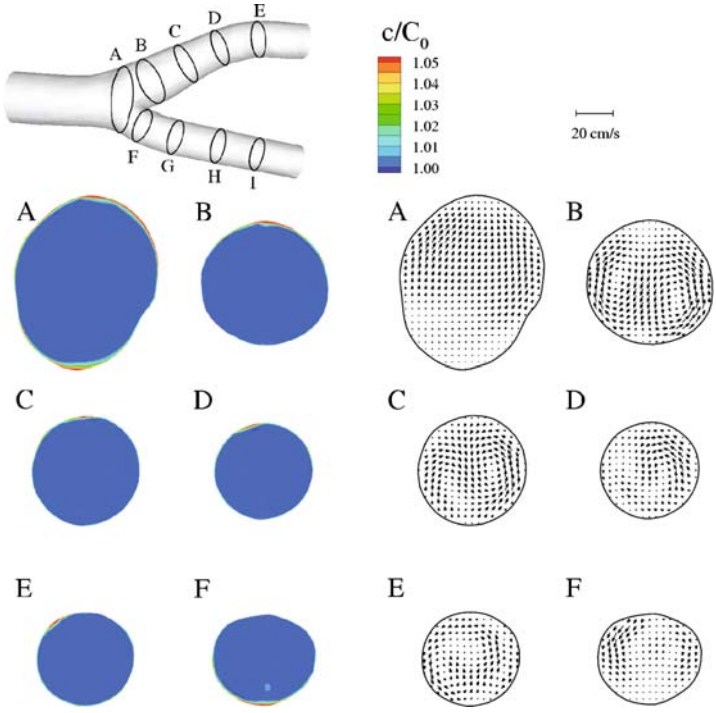

Fig. 7.13. Concentration contours of the LDL distribution and inplane motion in the arterial lumen at selected cross-sections in and downstream the bifurcation region

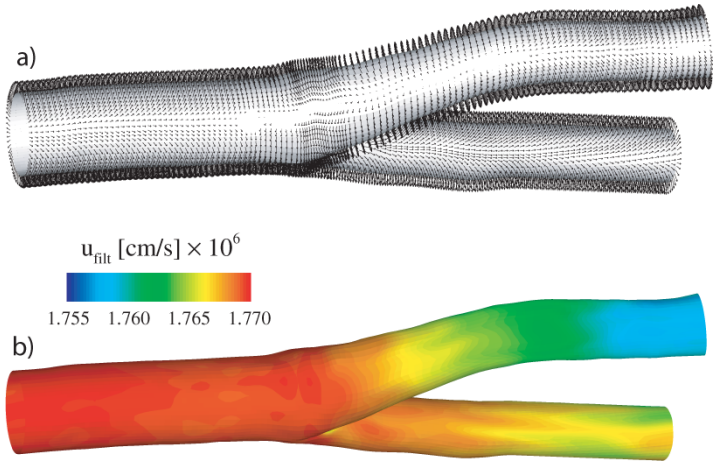

Fig. 7.14. Plasma filtration velocity field in the arterial wall at the interface membrane-wall, represented by means of vectors (a) and magnitude contours (b)

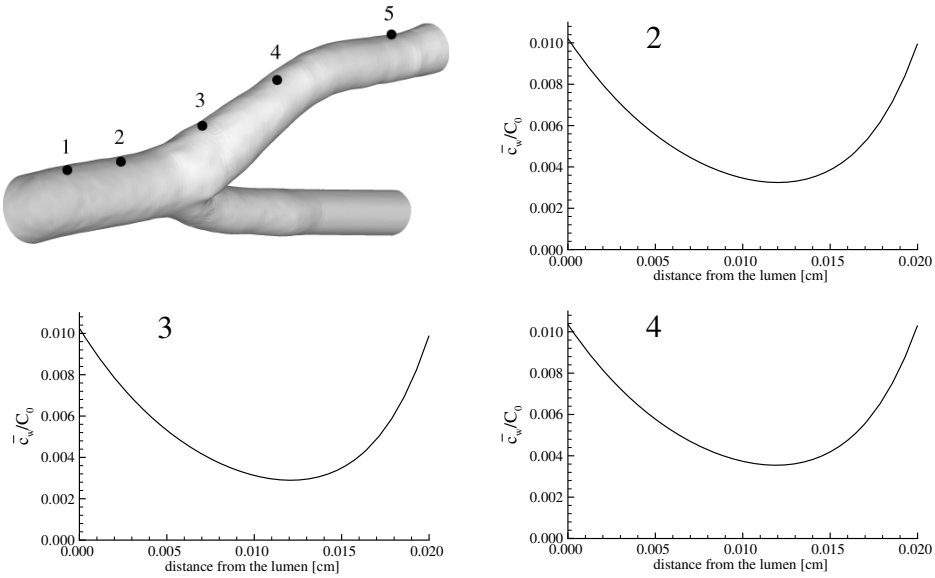

Fig. 7.15. Concentration profiles of the LDL-distribution at selected locations through the arterial wall

profiles are in good agreement with measured data of [49], [326] and suggest that the estimation method proposed in [397] provide suitable values of the transport parameters of the wall. Only small variation of LDL concentration at the membrane/wall side occurs due to the increased convective and diffusive transport in regions of high polarisation (point 3). This variation is small compared to the changes of concentration in normal direction caused by reaction of LDL with the wall tissue.

7.4.3 Numerical simulations of drug release from stents

A novel application of the mathematical models of mass transfer in the vascular walls is promoted by the introduction of drug eluting stents for the treatment of stenotic coronary arteries. Drug eluting stents (DES) are apparently simple medical implanted devices used to restore blood flow perfusion into stenotic arteries. Such structures are coated with a micro-film containing a drug that is locally released into the arterial walls for healing purposes. However, the design of such devices is a very complex task, because their performance in widening the arterial lumen and preventing further restenosis is influenced by many factors such as the geometrical design of the stent, the mechanical properties of the material and the chemical properties of the drug that is released. All these topics are relevant for an effective stent design. In this framework, numerical simulation techniques play a relevant role in under-

standing what are the most appropriate choices for the optimal design of DES. These topics will be addressed in detail in Chapter 12.

7.5 Conclusions

In this chapter we have proposed a possible way to set up suitable mathematical models with the aim to study the transfer of molecules, such as oxygen, macromolecules or drugs, through the arterial walls. A few recipes for their numerical discretisation have been considered. By means of these tools, we have addressed several applications and discussed their results in order to put into evidence the role of mass transfer in the physiological functions of the vascular system.